

COMPOSITION OF GYPSUM FROM THE KOBEŘICE QUARRY (CZECH REPUBLIC)

Pavel KONEČNÝ^{1)*}, Eva PLEVOVÁ¹⁾, Lenka VACULÍKOVÁ¹⁾, Alena KOŽUŠNÍKOVÁ¹⁾,
Janka PETERKOVÁ²⁾ and Marianna HUNDÁKOVÁ³⁾

¹⁾*Institute of Geonics, Academy of Sciences of the Czech Republic, v.v.i., Studentská 1768,
708 00 Ostrava, Czech Republic*

²⁾*GYPSTREND s.r.o. sádrovcové doly, 747 27 Kobeřice, Czech Republic*

³⁾*Technical University of Ostrava, 17. listopadu 15, 708 33, Ostrava, Czech Republic*

*Corresponding author's e-mail: konecpa@ugn.cas.cz

(Received November 2010, accepted June 2011)

ABSTRACT

This paper reports an investigation into the composition of gypsum from Kobeřice locality (Czech Republic). The X-ray diffraction along with FTIR spectroscopy and thermal analysis show that almost pure gypsum occurs mainly in autochthonous horizons. While allochthonous clastic deposition is represented by gypsum containing also calcite, quartz, clay minerals and organic matter.

KEYWORDS: Gypsum, Carpathian foredeep, Kobeřice, X-ray diffraction, FTIR spectroscopy, Thermal analysis

1. INTRODUCTION

Gypsum quarry in Kobeřice in Opava region is the only quarried gypsum deposit in Czech Republic. Evaporite sediments in this quarry belong to the westernmost part of the Carpathian Foredeep basin ranging from Moldova, Ukraine, Poland to the Czech Republic.

The history of exploitation of gypsum in Opava region begin in 1849, when the first gypsum mine was created in Municipal Park in Opava (Mátl, 1981). Kobeřice deposit was opened in years 1952 – 1956. Presently the exploitation is realized by GYPSTREND s.r.o. by quarrying in area of

approximately 600 000 m². The quarried material is used almost completely for plaster production.

GEOLOGY OF THE OPAVA BASIN

Opava basin is westernmost part of the eastern part of Carpathian Foredeep basin. It is a typical peripheral foreland basin filled with Miocene sediments (Fig. 1). These sediments are mainly deltaic and turbiditic siliciclastic deposits of Miocene age. In addition, evaporites of Early and Middle Miocene age occur in the Carpathian Foredeep (Rögl, 1999; Peryt, 2006).

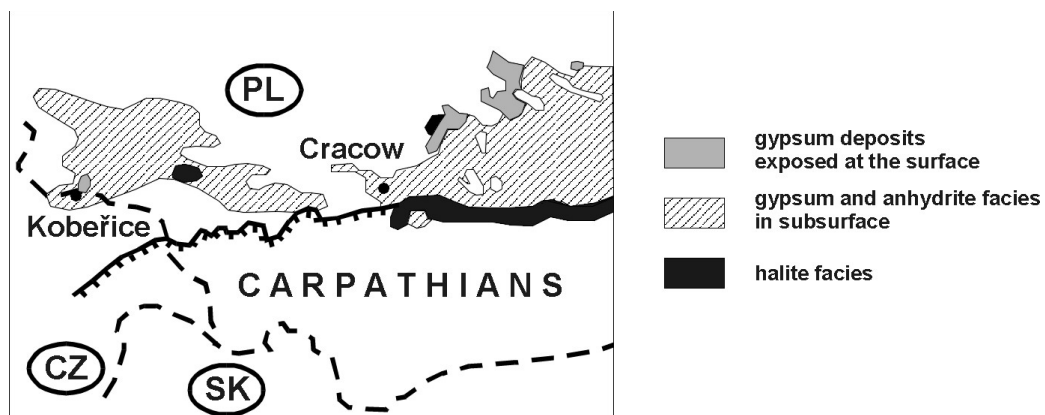


Fig. 1 Distribution of the gypsum deposits in the western part of Badenian (Middle Miocene) evaporite basin in the northern Carpathian Foredeep (after Babel, 2005, modified).

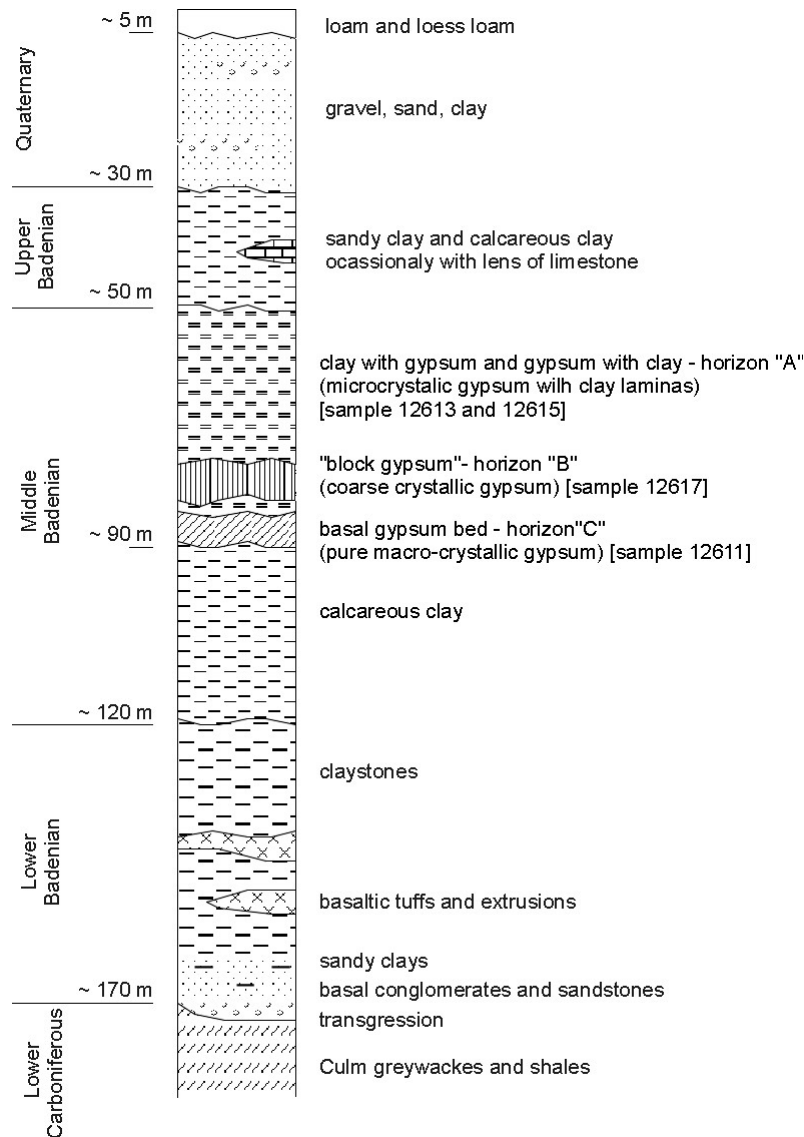


Fig. 2 Idealized stratigraphy column of Koberice gypsum quarry (after Mátl, 1981, modified).

Sedimentation in the Opava Basin began during Early Badenian times ("Lagenidae Zone") which corresponds to the Moravian regional substage (Piller et al., 2007), by transgression on the surface of weathered Culm (Lower Carboniferous) sedimentary rocks. Deposition of basal conglomerates was followed by sandy clays and claystones. Basaltic tuffs and rarely basaltic extrusions are recorded in these strata. The Early Badenian sedimentation continued during the Middle Badenian ("Spiroplectammina Zone") which corresponds to the Wielician substage when calcareous clays were deposited. During the final period of Middle Badenian sedimentation the evaporite formation with gypsum deposits originated (Fig. 2). The gypsum sequence of Koberice shows many similarities to other sequences known from the

marginal part of the Carpathian Foredeep basin (Peryt et al., 1997).

The lower gypsum complex ("C") is composed of macro-crystalline gypsum – giant gypsum intergrowths (Fig. 3) covered by clays (up to 1.7 m thick) and then by microcrystalline alabastrine gypsum (up to 0.3 m thick) (Peryt et al., 1997; Babel, 2005). This bottom-grown crystals form rows and thick beds and represent volumetrically one of the most important facies. Thickness of this gypsum bed is 1 to 9 m. The individual crystals of blocky crystalline intergrowths reach 2.5 m.

The middle complex ("B") is composed mostly of gypsum crystals which started to grow subhorizontally and then curved upward. These sabre crystals commonly developed syntaxially on the



Fig. 3 Giant bottom-grown gypsum crystals (complex “C”).

intergrowths, which are of the same crystallographic nature as the giant intergrowths from the complex “C”. The size of blocks of gypsum in gray clays is very variable and it is marked as “block gypsum”. The thickness of this sabre gypsum facies varies from 1 to 10m.

The most-upper horizon of evaporite sedimentation is 20 to 40m horizon “A”. Comparing the previous autochthonous evaporite horizons, this microcrystalline facies represents an environment dominated by allochthonous clastic deposition. The facies is composed mostly of the microcrystalline gypsum laminas and crystals making often a sedimentary breccia with the gray clays. Traces of bottom-grown halite crystals are common within the microcrystalline facies, too.

The evaporite horizon trace the surface of Culm fundament, thus the inclination of strata is very easy from 5 to 10°. Superincumbent bed is composed of Upper Badenian - “Bulimina/Bolivina Zone” (corresponding to substage Kosovian) clays or calcareous clays (Fajkus and Mátl, 1976). Quarternary glacial sediments and loam make the uppermost part of superincumbent bed.

2. SAMPLES AND METHODS

2.1. TESTED MATERIAL

The evaporite sediments occur in several petrological characters forming a different facies. Four varieties of gypsum representing different gypsum facies were selected for analysis. Selected macro-petrographical types are shown in Table 1.

Table 1 Selected macro-petrographical types.

<i>Number of the sample</i>	<i>Macropetrographic type</i>	<i>Stratigraphy</i>
12613	gypsum with grey clay	horizon “A”
12615	laminated gypsum	horizon “A”
12617	gypsum crystal	horizon “B”
12611	alabastrine	horizon “C”



Fig. 4 Photomicrograph of scattered alabastrine crystals – sample 12611 (confocal microscopy; laser).

Grey clay with fine grained gypsum (12613) and sedimentary breccia with microcrystalline gypsum laminated with clays (12615) occur mostly in horizon “A” as a result of allochthonous sedimentation.

Gypsum crystals (12617) create grass-like facies in horizon “C”, and sabre crystals typical for bed “B”. The shape of the crystals is elongated, color is greyish to orange mostly translucent creating intergrowth of different shape and size.

Layer of alabastrine (12611) is typical with white coloration and very fine microcrystalline structure. Microstructure of this material is shown in Figure 4.

2.2. METHODS OF ANALYSIS

X-RAY DIFFRACTION

X-ray diffraction (XRD) was performed by using Bruker D8 Advance X-ray powder diffractometer. XRD patterns were obtained using position sensitive Vantec detector, Co K_{α} radiation and working conditions 35 kV and 25 mA, 0.03° 2θ increment and time at step 1s. The presence of individual phases was evaluated by software ICCD 2004 (EVA) with an extensive database of minerals and other inorganic substances.

FTIR SPECTROSCOPY

Infrared spectra were recorded on Nicolet Avatar 320 FTIR spectrometer equipped with a DTGS/KBr detector. The KBr pressed-disk technique (2 mg of sample and 200 mg of KBr) was used. The spectra

were measured by accumulating 64 scans at 4 cm^{-1} resolution in the spectral range from 4,000 to 400 cm^{-1} . The measured IR spectra were compared with records of published data and spectra (Farmer, 1974; Van der Marel and Beutelspracher, 1976; Vaculíková and Plevová, 2005).

SIMULTANEOUS THERMOGRAVIMETRY AND DIFFERENTIAL THERMAL ANALYSIS

Thermal properties were investigated by simultaneous thermogravimetry and differential thermal analysis using the thermal analyzer Setsys 12 Setaram with thermal measurement head TG ATD Rod. The TG/DTA curves were recorded in air atmosphere with a heating rate $10\text{ }^{\circ}\text{C min}^{-1}$ to the final temperature $1000\text{ }^{\circ}\text{C}$. The sample mass was about 50 mg. Thermal analysis was used to both complete the composition evaluation (Smykatz-Kloss, 1974; Hatakeyama and Liu, 1998) and determine gypsum and carbonate content in test samples corresponding to (Gabbott, 2008; Plevová et al., 2010).

3. RESULT AND DISCUSSION

X-ray diffraction along with FTIR spectroscopy and thermal analysis gave the information of sample composition summarized below.

SAMPLE 12613

X-ray diffraction analysis was used to evaluate patterns considering the phase analysis. XDR pattern showed, that sample 12613 contained predominantly

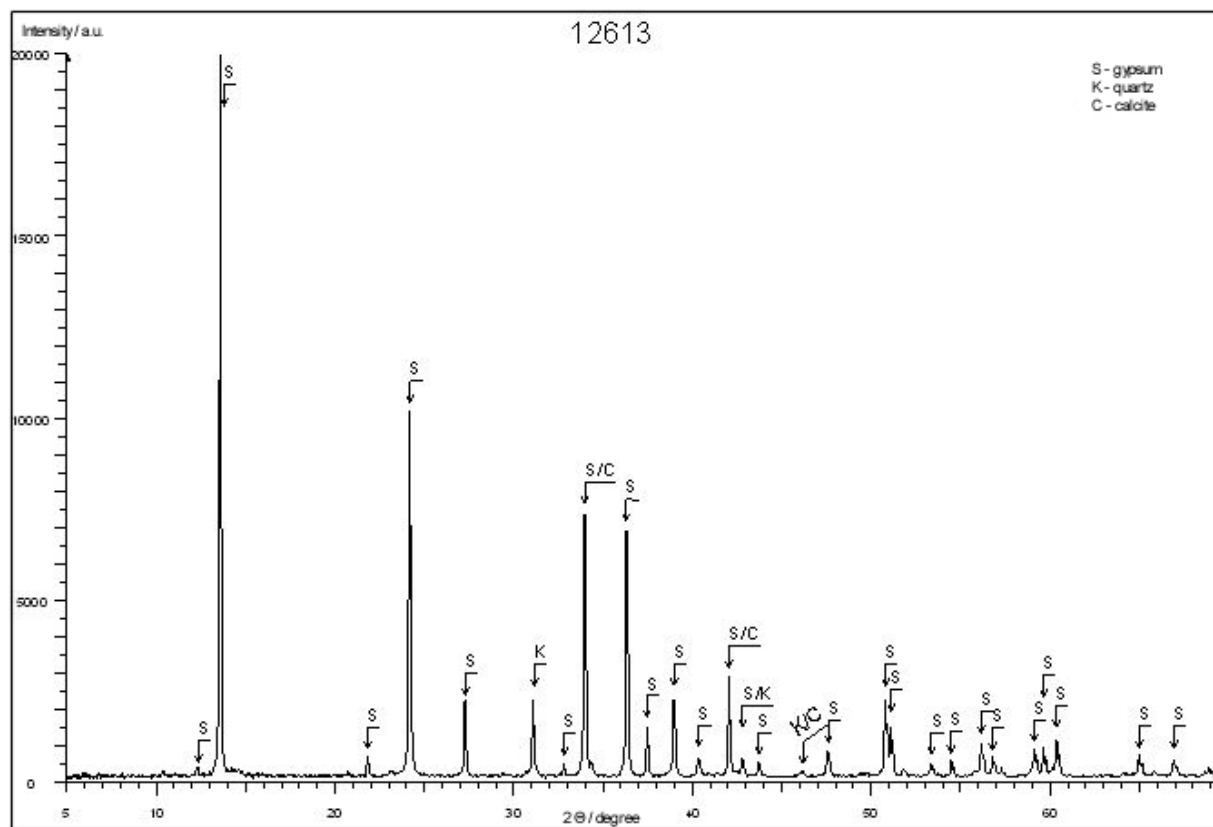


Fig. 5 XRD pattern of sample 12613.

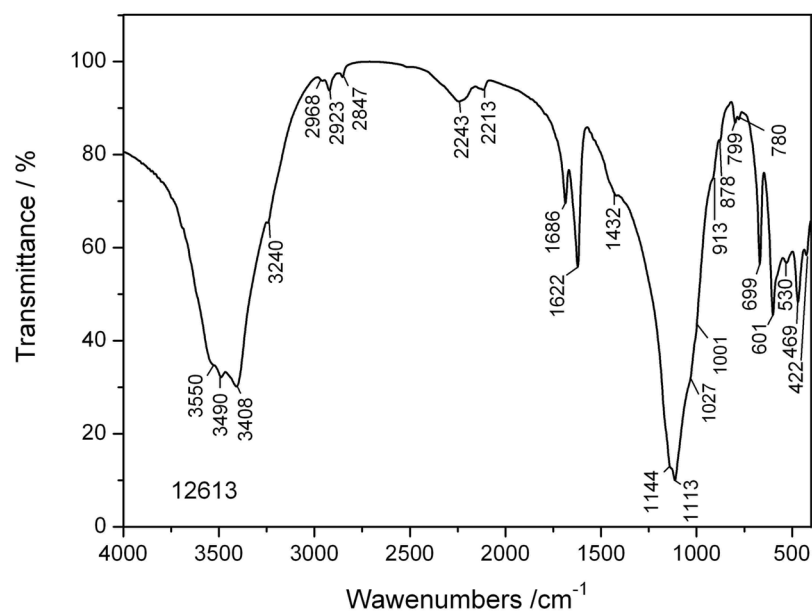


Fig. 6 FTIR spectrum of sample 12613.

gypsum and small amount of quartz and calcite (Fig. 5). FTIR spectrum (Fig. 6) showed the presence of predominant component gypsum (main absorption bands at 3550, 3490, 3408, 3240, 2243, 2113, 1686, 1622, 1144, 1113, 669, 601, 469 cm^{-1}).

The quartz (absorption bands at 799 and 780 cm^{-1}), calcite (1435, 878 cm^{-1}) and illite/smectite (1027, 1001, 913 cm^{-1}) were observed as traces. DTA curves showed the presence of gypsum, which dehydrated in two stages with relevant endothermic effects at 158 and 191 $^{\circ}\text{C}$.

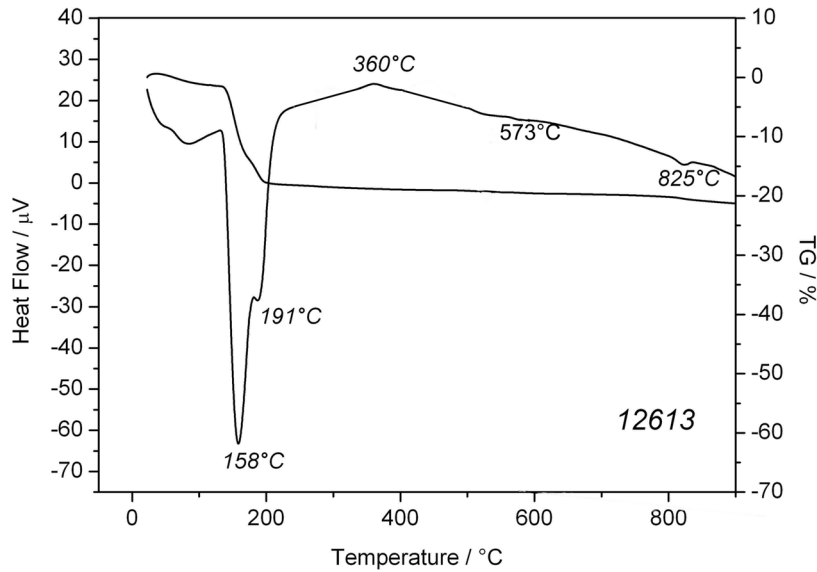


Fig. 7 TG/DTA curves of sample 12613.

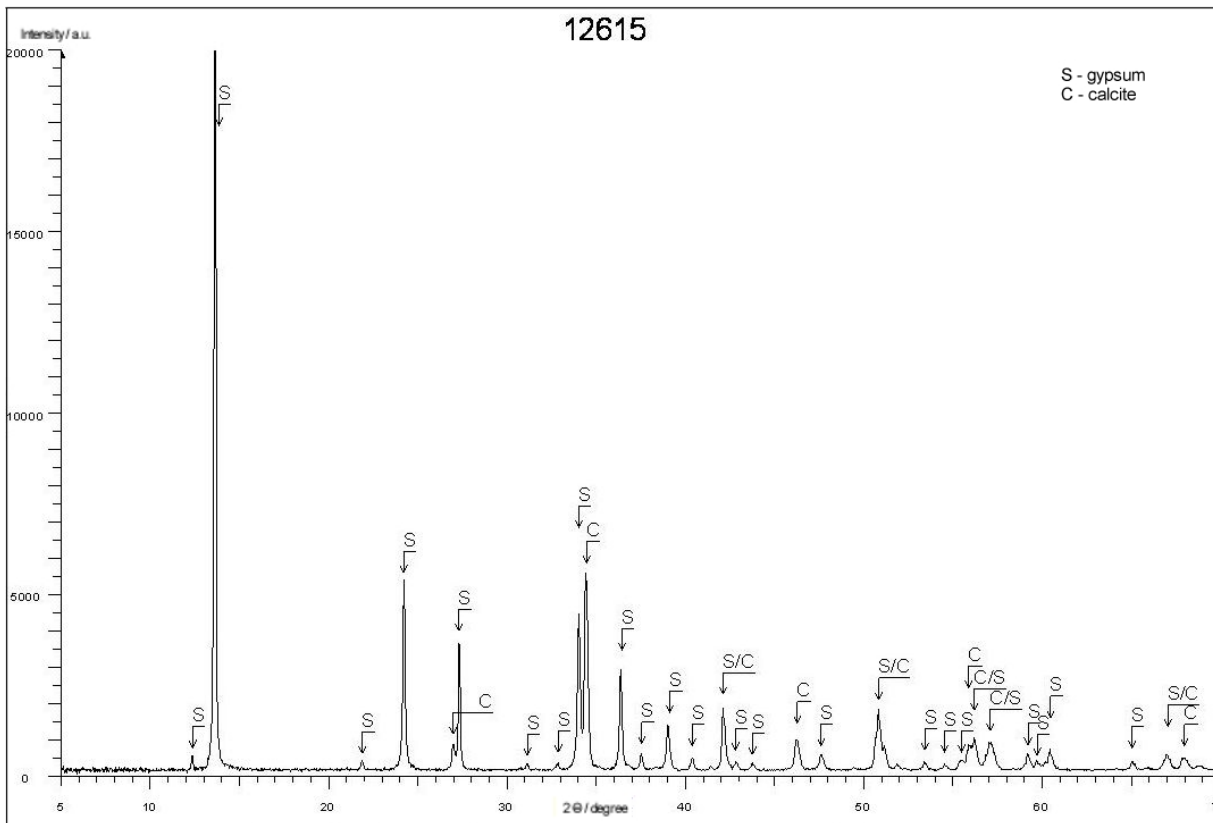


Fig. 8 XRD pattern of sample 12615.

At 360 °C, CaSO_4 crystallized and formed anhydrite with relevant exothermic effect. DTA curves showed also presence of quartz traces according to endotherm peak corresponding with α - β modification at 573 °C, presence of clay according to flat endothermic effect at about 530 °C accompanied by mass loss and calcite traces with endotherm peak at 825 °C (Fig. 7).

SAMPLE 12615

According to XRD pattern, sample 12615 contained two components, gypsum and calcite (Fig. 8). According to FTIR measurements, sample contained gypsum (main absorption bands at 3546, 3487, 3405, 3240, 2246, 2113, 1685, 1621, 1141, 1112, 669, 602, 470 cm^{-1}), calcite (main absorption

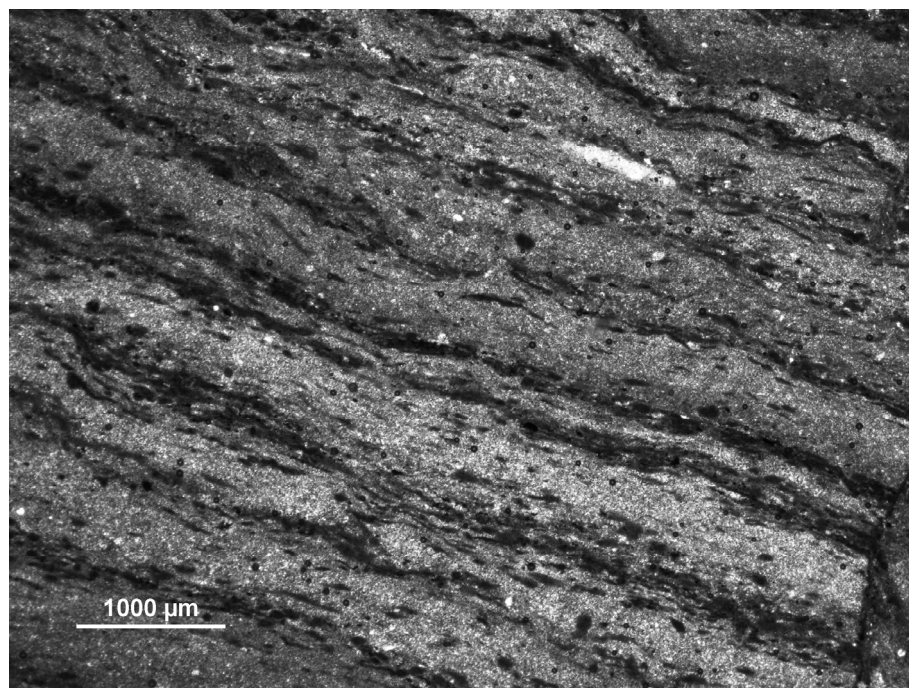


Fig. 9 Photomicrograph of the micro laminas and lenses of organic matter – sample 12615 (transmitted light, crossed polars).

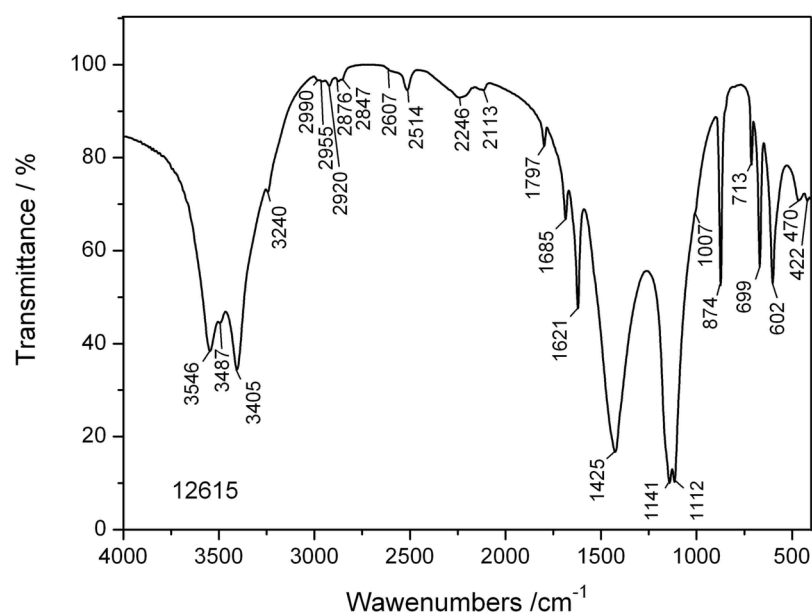


Fig. 10 FTIR spectrum of sample 12615.

bands at 2514, 1797, 1425, 874, 713 cm^{-1}) and organic traces (low intensity absorption bands ranged from 2990 to 2847 cm^{-1}). The presence of dark laminas of organic matter was also confirmed by microscopic analysis of thin section. (Fig. 9). For illustrative purposes, FTIR spectrum is given in Figure 10. Thermal analysis confirmed the presence of gypsum

(endotherm peaks at 151 °C and 180 °C, exotherm peak at 359 °C). Calcite was detected according to endotherm peak at 885°C (decomposition to CaO and CO_2). Small exothermic peak at 420 °C showed the possibility of organic matter presence. TG/DTA curves are shown in Figure 11.

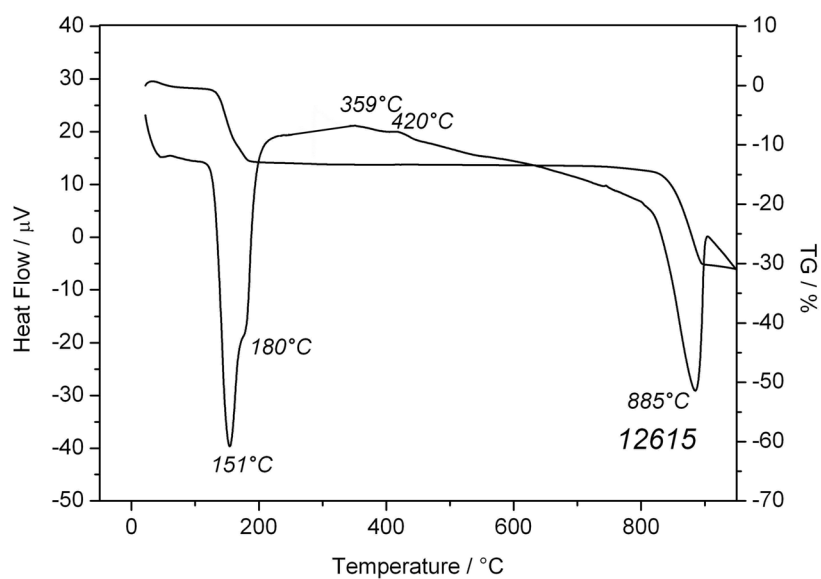


Fig. 11 TG/DTA curves of sample 12615.

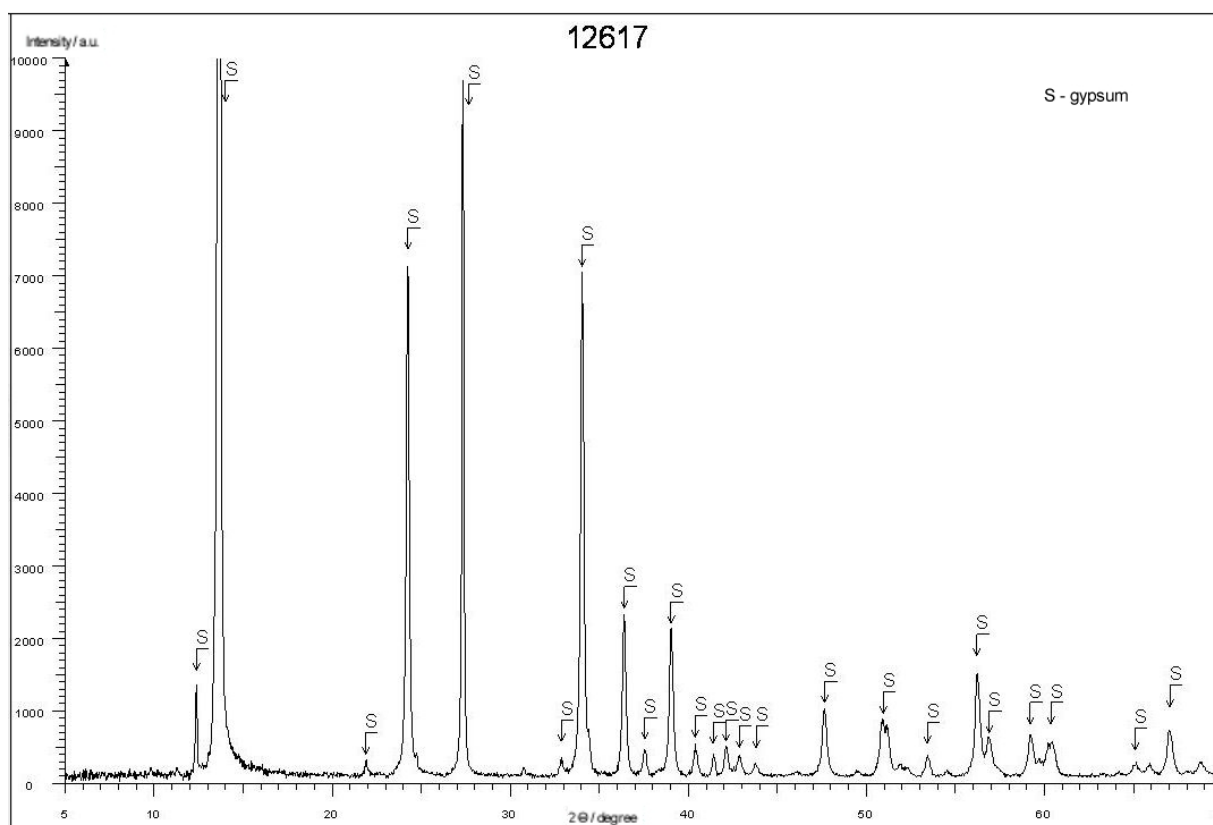


Fig. 12 XRD pattern of sample 12617.

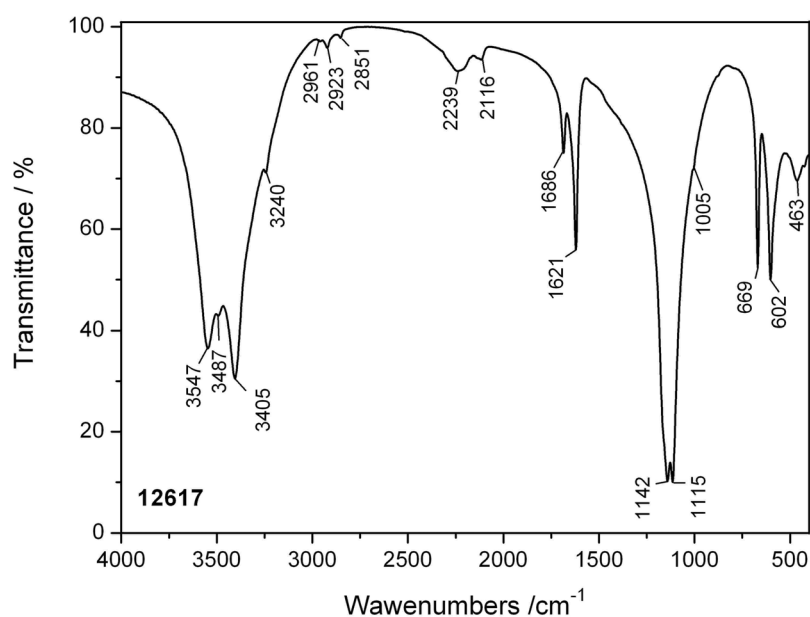


Fig. 13 FTIR spectrum of sample 12617.

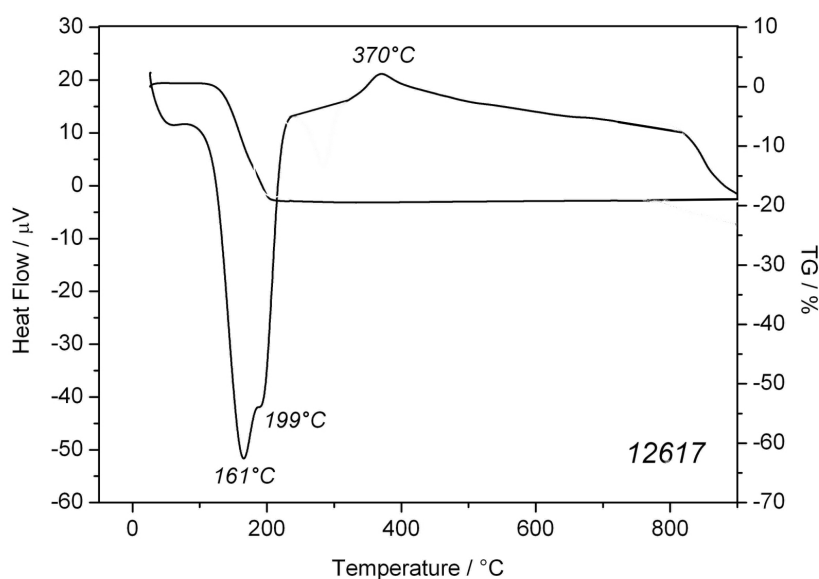


Fig. 14 TG/DTA curves of sample 12617.

SAMPLE 12617

XRD patterns showed, that gypsum was the only component in sample 12617 (Fig. 12). FTIR spectroscopy also detected only gypsum (main absorption bands at 3547, 3487, 3405, 3240, 2239, 2116, 1686, 1621, 1142, 1115, 669, 602 cm^{-1}). For illustrative purposes, FTIR spectrum is given in Figure 13. DTA curves showed the presence of gypsum (endothermic effects at 161 °C and 199 °C). At 370 °C, CaSO_4 crystallized and formed anhydrite with relevant exothermic effect (Fig. 14).

SAMPLE 12611

In sample 12611, gypsum was found as the main component according to XRD patterns (Fig. 15). FTIR spectra (Fig. 16) confirmed the presence of gypsum (main absorption bands at 3547, 3487, 3406, 3243, 2241, 2113, 1687, 1621, 1144, 1114, 669, 601 cm^{-1}). The traces of amorphous SiO_2 were detected by absorption band at 796 cm^{-1} . DTA curves showed the presence of gypsum (dehydration at 163 °C and 195 °C, anhydrite formation at 362 °C). At 573 °C was found a small wider peak corresponding probably with the presence of bad crystal form of SiO_2 (Fig. 17). The presence of SiO_2 could not be confirmed by X-ray diffraction because of its amorphous state.

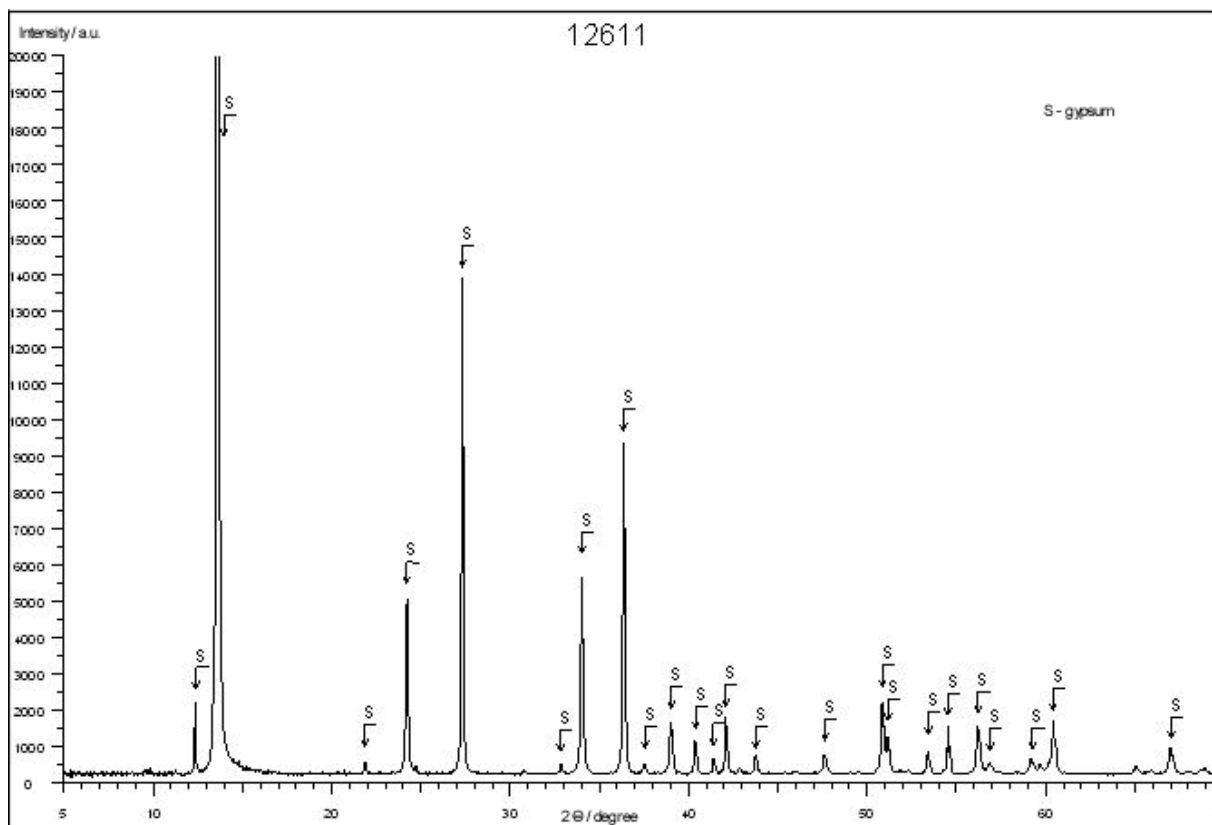


Fig. 15 XRD pattern of sample 12611.

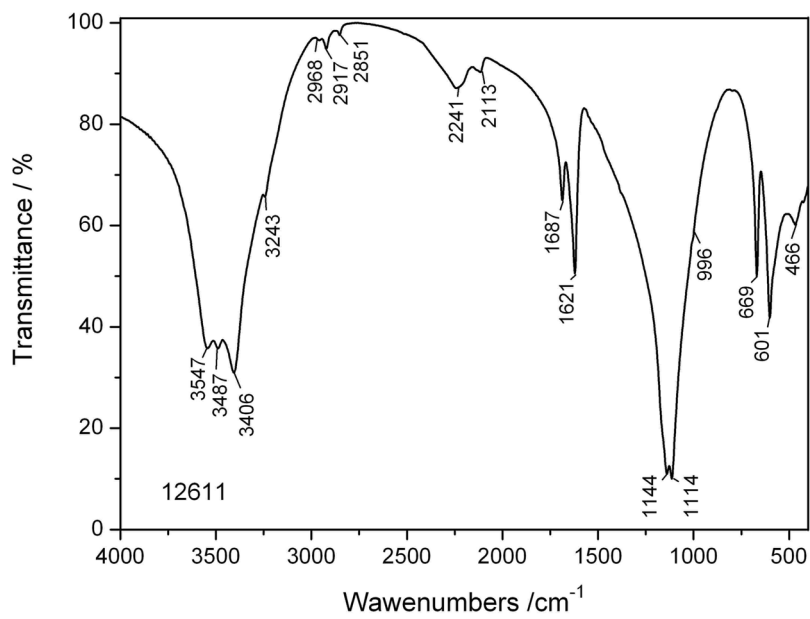


Fig. 16 FTIR spectrum of sample 12611.

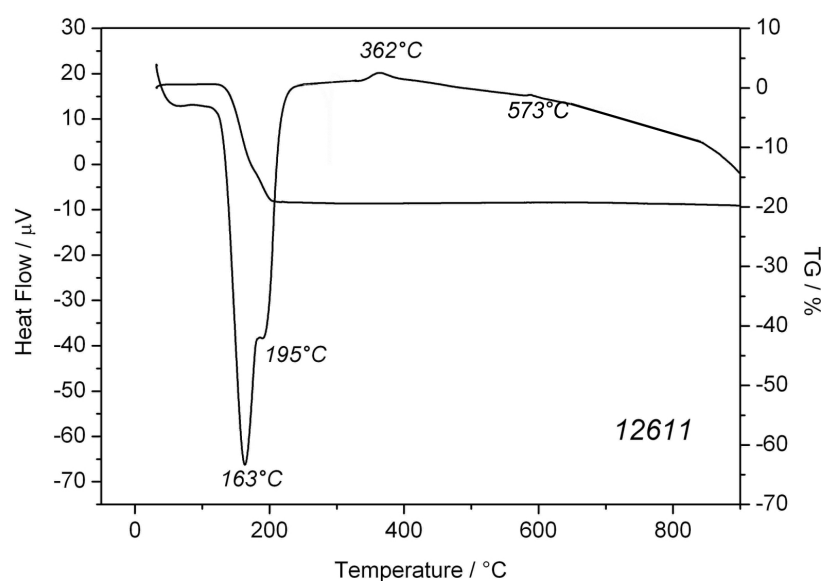


Fig. 17 TG/DTA curves of sample 12611.

Table 2 Thermal data including average gypsum (G_G) and carbonate (G_C) content.

Sample	G_G (%)	G_C (%)
12611	85	-
12613	70	8
12615	50	45
12617	90	-

The summary of results obtained from TG curves (the average gypsum content (G_G) and carbonate content (G_C)) - average determination of five measurements is shown in Table 2.

4. CONCLUSIONS

The measurements performed on selected samples confirmed that gypsum is the main mineral in Kobeřice deposits. The almost pure gypsum occurs mainly as a macro-crystalline gypsum, grass-like crystals or alabastrine occurring in autochthonous horizons.

Laminated microcrystalline breccia, typical for allochthonous horizons, in addition to gypsum contains also calcite, quartz, clay minerals and organic matter. The quantity of calcite can exceed 40 % in some cases. The presence of these minerals can strongly affect the final properties of quarried raw material.

ACKNOWLEDGEMENTS

This study was supported by the Czech Science Foundation, the project No.105/08/1398 and No.105/07/P416, and by Research plan No. AVOZ 30860518. The authors would like to thank George Laynr for controlling and correcting the use of English in this article.

REFERENCES

- Babel, M.: 2005, Selenite-gypsum microbialite facies and seimentary evolution of the Badenian evaporite basin of the northern Carpathian Foredeep. *Acta Geologica Polonica*, 55, 187–210.
- Fajkus, O. and Mátl, V.: 1976, Gypsum deposits in Opava region and their exploitation. *Sborník GPO*, 12, 77–86, (in Czech).
- Farmer, V.C.: 1974, *The infrared spectra of minerals*. Mineralogical Society, London.
- Gabbott, P.: 2008, *Principles and applications of thermal analysis*, Blackwell Publishing.
- Hatakeyama, T. and Liu, Z.: 1998, *Handbook of thermal analysis*, Wiley, New York.

- Mátl, V.: 1981, Gypsum deposits of Opava Basin. 12, 346–350, (in Czech).
- Peryt, T.M., Karol, S., Peryt, D., Petrichenko, O.I., Gedl, P., Narkiewicz, W., Ďurkovičová, J. and Dobieszyńska, Z.: 1997, Westernmost occurrence of the Middle Miocene Badenian gypsum in central Paratethys (Kobeřice, Moravia, Czech Republic). *Slovak Geol. Mag.*, 3, 105–120.
- Peryt, T.M.: 2006, The beginning, development and termination of the Middle Miocene Badenian salinity crisis in Central Paratethys. *Sedim. Geol.*, 188–189, 379–396.
- Piller, W.E., Harzhauser, M. and Mandic, O.: 2007, Miocene Central Paratethys stratigraphy – current status and future directions. *Stratigraphy*, 4, 151–168.
- Plevová, E., Kožušnicková, A., Vaculíková, L. and Simha Martynková, G.: 2010, Thermal behavior of selected Czech marble samples. *Journal of Thermal Analysis and Calorimetry*, 101, 2, 657–664.
- Rögl, F.: 1999, Mediterranean and Paratethys. Facts and hypotheses of an Oligocene to Miocene paleogeography (short overview). *Geologica Carpathica*, 50, 339–349.
- Smykatz-Kloss, W.: 1974, *Differential thermal analysis: application and results in mineralogy*, Springer-Verlag, Berlin.
- Van der Marel, M.J. and Beutelspracher H.: 1976, *Atlas of infrared spectroscopy of clay minerals and their admixtures*, Elsevier.
- Vaculíková, L. and Plevová, E.: 2005, The identification of clay minerals and micas in sedimentary rocks. *Acta Geodyn. Geomater.*, 2 (2), 163–175.